Püthe *et al. Earth, Planets and Space* (2014) 66:162
DOI 10.1186/s40623-014-0162-2

Earth, Planets and Space
a SpringerOpen Journal

FULL PAPER Open Access

Reproducing electric field observations during magnetic storms by means of rigorous 3-D modelling and distortion matrix co-estimation

Christoph Püthe[1*], Chandrasekharan Manoj[2] and Alexey Kuvshinov[1]

Abstract

Electric fields induced in the conducting Earth by geomagnetic disturbances drive currents in power transmission grids, telecommunication lines or buried pipelines, which can cause service disruptions. A key step in the prediction of the hazard to technological systems during magnetic storms is the calculation of the geoelectric field. To address this issue for mid-latitude regions, we revisit a method that involves 3-D modelling of induction processes in a heterogeneous Earth and the construction of a magnetospheric source model described by low-degree spherical harmonics from observatory magnetic data. The actual electric field, however, is known to be perturbed by galvanic effects, arising from very local near-surface heterogeneities or topography, which cannot be included in the model. Galvanic effects are commonly accounted for with a real-valued time-independent distortion matrix, which linearly relates measured and modelled electric fields. Using data of six magnetic storms that occurred between 2000 and 2003, we estimate distortion matrices for observatory sites onshore and on the ocean bottom. Reliable estimates are obtained, and the modellings are found to explain up to 90% of the measurements. We further find that 3-D modelling is crucial for a correct separation of galvanic and inductive effects and a precise prediction of the shape of electric field time series during magnetic storms. Since the method relies on precomputed responses of a 3-D Earth to geomagnetic disturbances, which can be recycled for each storm, the required computational resources are negligible. Our approach is thus suitable for real-time prediction of geomagnetically induced currents by combining it with reliable forecasts of the source field.

Keywords: Magnetic storms; Geomagnetically induced currents; Geoelectric field; Static shift; Distortion matrix; 3-D modelling

Background

Electric fields induced in the conducting Earth by geomagnetic disturbances drive currents in power transmission grids, telecommunication lines or buried pipelines. These currents, known as geomagnetically induced currents (GIC), are known to cause service disruptions (e.g. Daglis 2004, and references therein). The effect is maximal at high latitudes due to the presence of strong polar electrojet currents (e.g. Pulkkinen et al. 2012; Viljanen and Pirjola 1994). However, both observations and models show that massive GIC caused by intensifications of the magnetospheric ring current also pose a risk at low- and mid-latitudes, where the majority of systems vulnerable to GIC are located (e.g. Kappenman 2005).

A technique to model the geoelectric field induced by large-scale magnetospheric currents in a 3-D conductivity model of the Earth was presented by Püthe and Kuvshinov (2013), based on a previous study by Olsen and Kuvshinov (2004). The authors used precomputed electromagnetic (EM) responses of the 3-D model and magnetic data from the global network of geomagnetic observatories to construct the magnetospheric source, described by spherical harmonic expansion (SHE) coefficients. A convolution of the source with the precomputed model responses yielded time series of electric and magnetic fields anywhere on the surface of the Earth.

*Correspondence: christoph.puethe@erdw.ethz.ch
[1] Institute of Geophysics, ETH Zürich, Sonneggstrasse 5, 8092 Zürich, Switzerland
Full list of author information is available at the end of the article

The methodology of Püthe and Kuvshinov (2013) is self-consistent, but depending on location, the presented results might still over- or underestimate the amplitudes of the actual electric field. This is due to galvanic effects, i.e. the build-up of electric charges along near-surface, small-scale conductivity contrasts or topographic inhomogeneities (e.g. Jiracek 1990) that were not included in the model. Galvanic effects are well-known in the magnetotelluric (MT) community, where they are usually referred to as 'static shift' (e.g. Chave and Jones 2012; Simpson and Bahr 2005). This name reflects the frequency-independent shift of MT response functions (apparent resistivities) that the effect causes. MT responses are routinely corrected for the static shift by introducing a real-valued frequency-independent distortion matrix, which separates galvanic from (the usually desired) inductive effects (e.g. Groom and Bahr 1992).

Little galvanic effects are expected on the bottom of oceanic basins due to the relatively homogeneous deposit of deep-sea sediments and the consequential layered structure. By analysing data from an ocean bottom MT survey in the Philippine Sea, we in this paper first validate the concept of Püthe and Kuvshinov (2013). We then analyse electric field data at onshore geomagnetic observatories in Japan for six magnetic storms. By relating model predictions to the measurements, we estimate the distortion matrix for each observatory. Statistical inferences are drawn from a comparison of the results obtained for different storms. With help of the estimated distortion matrices, we finally show how our concept can be applied to real-time prediction of the electric field during magnetic storms.

Methods

In this section, we first give an overview of the data used in the present study. We then briefly review the methodology presented in more detail by Püthe and Kuvshinov (2013) before outlining the estimation of distortion matrices.

Data

Earth's magnetic field is routinely measured at more than 150 geomagnetic observatories worldwide, of which, as this paper is written, about 120 are part of the International Real-Time Magnetic Observatory Network INTERMAGNET (Love and Chulliat 2013). We collect minute mean definitive vector data of all available observatories at geomagnetic latitudes equatorward of $\pm 55°$ for in total six magnetic storms. All storms occurred during the peak phase of solar cycle 23, namely in April 2000, July 2000, August 2000, March 2001, October 2003 and November 2003. For each storm, we select a time segment of 10 days, covering build-up phase, main phase and recovery phase. A summary of the data is given in Table 1. The magnetic data are used to construct a model of the magnetospheric source, as will be described in the next subsection.

Table 1 Overview of the magnetic data used in this study

Storm	*Dst*	Start date/UTC	End date/UTC	Observatories
Apr-2000	−288	00/04/03 14:00	00/04/13 14:00	56
Jul-2000	−301	00/07/12 18:00	00/07/22 18:00	65
Aug-2000	−235	00/08/09 00:00	00/08/19 00:00	63
Mar-2001	−387	01/03/28 00:00	01/04/07 00:00	63
Oct-2003	−388	03/10/26 12:00	03/11/05 12:00	70
Nov-2003	−422	03/11/17 00:00	03/11/27 00:00	72

The second column contains the peak *Dst* values for each storm. The last column contains the number of observatories from which data were used to construct the source field model.

While long-term measurements of the geomagnetic field at observatories are common, the geoelectric field is usually only measured in MT field campaigns. The Japanese observatories Kakioka (KAK), Kanoya (KNY) and Memambetsu (MMB), all part of INTERMAGNET, are an exception, as all of them have routinely measured the geoelectric field for several decades (Minamoto 2013). We use minute mean electric field data of all three observatories to estimate distortion matrices, as outlined below.

In addition, we use minute mean electric field data from an ocean bottom MT survey, carried out from November 1999 to July 2000 in the Philippine Sea (Seama et al. 2007). The survey was based on six ocean bottom electromagnetometers, deployed along a line at water depths between 3,250 and 5,430 m. The stations in particular recorded the April 2000 magnetic storm and are thus of interest for our analysis. The observatories and ocean bottom electro-magnetometers providing electric field data are depicted on a map in Figure 1.

We subtract the baseline and a linear trend from both magnetic and electric data to remove main field contributions and possible instrument drift. All magnetic data are checked visually for gaps and offsets; small gaps are interpolated and channels with low-quality data or large gaps are removed.

Calculation of the electric field

EM fields obey Maxwell's equations. We formulate them in frequency domain as

$$\frac{1}{\mu_0}\nabla \times \mathbf{B} = \sigma \mathbf{E} + \mathbf{j}^{\text{ext}}, \tag{1}$$

$$\nabla \times \mathbf{E} = \mathrm{i}\omega \mathbf{B}. \tag{2}$$

Here, $\mathbf{B}(\mathbf{r}, \omega)$ and $\mathbf{E}(\mathbf{r}, \omega)$ are the complex Fourier transforms of magnetic flux density and electric field, respectively, and $\mathbf{j}^{\text{ext}}(\mathbf{r}, \omega)$ is the complex Fourier transform of

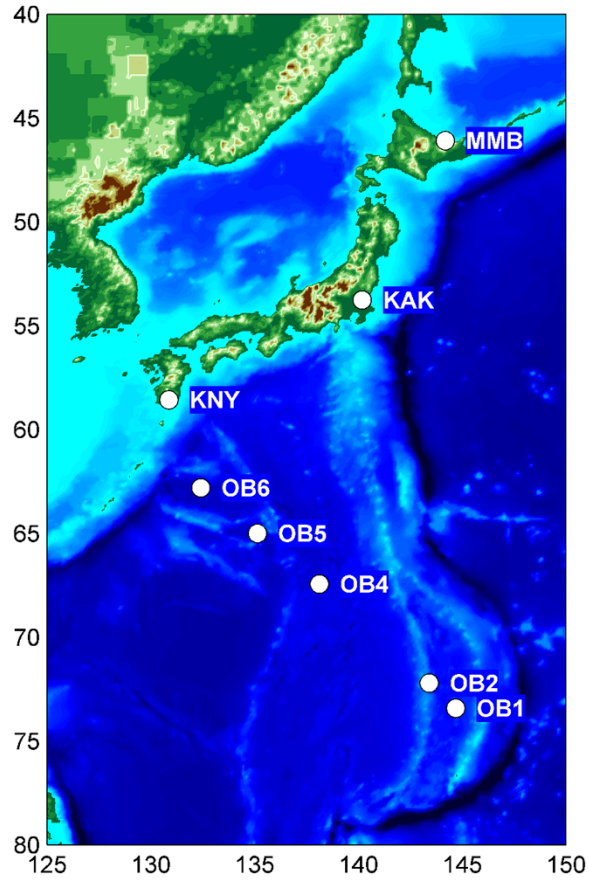

Figure 1 E-field measurement sites. The three Japanese observatories provide electric field data continuously, whereas the ocean bottom array was installed during the April 2000 magnetic storm. Note that OB3, which was installed on the seafloor between OB2 and OB4, did not provide useful data. Colours indicate topography/bathymetry.

the electric current density of the inducing source. The position vector $\mathbf{r} = (r, \vartheta, \varphi)$ describes a spherical coordinate system, with r, ϑ and φ being the distance from the Earth's centre, colatitude and longitude, respectively. Further, $\sigma(\mathbf{r})$ is the spatial conductivity distribution in the Earth, ω denotes angular frequency and μ_0 is the magnetic permeability of free space. Our formulation of Maxwell's equations discards displacement currents, which are negligible in the frequency range considered here.

Equation 1 illustrates that electric and magnetic fields are linear with respect to the source. This means that the total electric and magnetic fields can be represented as the sum of individual electric and magnetic fields due to specific sources. We parametrize the source field $\mathbf{j}^{\text{ext}}$ with spherical harmonics Y_n^m (where n and m denote degree and order of the spherical harmonic, respectively), as demonstrated in Appendix G of Kuvshinov and Semenov (2012). This allows us to write electric and magnetic fields outside the source region as

$$\mathbf{B}(\mathbf{r},\omega) = \sum_{n=1}^{\infty}\sum_{m=-n}^{n} \varepsilon_n^m(\omega)\mathbf{B}_n^{m,\text{unit}}(\mathbf{r},\omega), \tag{3}$$

$$\mathbf{E}(\mathbf{r},\omega) = \sum_{n=1}^{\infty}\sum_{m=-n}^{n} \varepsilon_n^m(\omega)\mathbf{E}_n^{m,\text{unit}}(\mathbf{r},\omega), \tag{4}$$

where $\mathbf{B}_n^{m,\text{unit}}$ and $\mathbf{E}_n^{m,\text{unit}}$ are EM responses of the Earth due to unit scale spherical harmonic sources, respectively. The factors ε_n^m are the SHE coefficients describing the frequency content of the inducing source. Note that in practice, the double sums in Equations 3 and 4 are finite.

The calculation of electric field time series during a magnetic storm involves the following steps:

1. Calculation of $\mathbf{B}_n^{m,\text{unit}}$ and $\mathbf{E}_n^{m,\text{unit}}$ in a 3-D conductivity model for the desired set of spherical harmonic sources and representative frequencies ω. This is done using a contracting integral equation approach (Kuvshinov 2008). The responses are modelled at Earth's surface on a regular $1° \times 1°$ mesh.
2. Spatial interpolation of $\mathbf{B}_n^{m,\text{unit}}$ to observatory locations $\mathbf{r}_j$.
3. Interpolation of $\mathbf{B}_n^{m,\text{unit}}$ to the full set of frequencies contained in the data.
4. Fourier transformation of observed time series $\mathbf{B}^{\text{obs}}(\mathbf{r}_j, t)$, yielding $\mathbf{B}^{\text{obs}}(\mathbf{r}_j, \omega)$.
5. For each frequency ω, construction of a system of linear equations (Equation 3) and solution of this system for coefficients $\varepsilon_n^m(\omega)$ using iteratively re-weighted least squares (e.g. Aster et al. 2005). Only the horizontal components of $\mathbf{B}$ are used, since they are less influenced by conductivity heterogeneities than B_r (as demonstrated by Olsen and Kuvshinov 2004).
6. Interpolation of $\mathbf{E}_n^{m,\text{unit}}$ to the full set of frequencies contained in the data.
7. Calculation of $\mathbf{E}(\mathbf{r},\omega)$ at any observation point by means of Equation 4.
8. Inverse Fourier transformation of $\mathbf{E}(\mathbf{r},\omega)$, yielding time series $\mathbf{E}(\mathbf{r},t)$.

Details of this scheme are given in Püthe and Kuvshinov (2013). It is noteworthy that the time-consuming solution of Maxwell's equations in a global 3-D conductivity model (step 1) only has to be done once; the results can be recycled for every storm under investigation. Also note that the same scheme with modified steps 6 to 8 can be used to consistently reproduce time series of B_r, as done by Olsen and Kuvshinov (2004).

Conductivity model

The 3-D conductivity model we use for our study consists of a laterally heterogeneous surface shell (with a resolution of 1°) and a layered 1-D structure underneath. The surface shell (taken from Manoj et al. 2006) accounts for the distribution of oceans and continents as well as sediment thicknesses. The resistivity of the lithosphere, extending from the surface shell to a depth of 100 km, is fixed to 3,000 Ωm. At greater depths, we use the conductivity model recovered by Kuvshinov and Olsen (2006) from 5 years of CHAMP, Ørsted and SAC-C magnetic data. The conductivity model is depicted in Figure 2.

Our model neglects conductivity heterogeneities at depths greater than 10 km. There is an ongoing project (Alekseev et al. 2014) that aims at compiling a more sophisticated 3-D model, which represents structures in the depth range of 0 to 100 km, including seawater, sediments, crust and partly lithosphere/asthenosphere. Once available, this model can readily be incorporated into our algorithm.

Estimation of distortion matrices

Let us first, for convenience, define a local Cartesian coordinate system at each observatory, with $E_x = -E_\vartheta$ pointing north and $E_y = E_\varphi$ pointing east. The radial electric field vanishes at the Earth's surface, since air is assumed to be insulating. We therefore restrict ourselves from here on to the horizontal electric field and redefine $\mathbf{E} = (E_x, E_y)^\top$.

Electric charges accumulate along conductivity contrasts. Such a charge build-up at small-scale heterogeneities, often located near the surface, generates a local quasi-static electric field, which is barely related to the electric field due to regional-scale induction (e.g. Jiracek 1990). In the MT community, this effect is referred to as galvanic distortion. The Fourier transforms of the theoretical/modelled electric field (purely due to inductive effects) $\mathbf{E}^{\mathrm{mod}}(\omega)$, and the actual measured/observed field $\mathbf{E}^{\mathrm{obs}}(\omega)$ are then related as (e.g. Chave and Jones 2012; Groom and Bahr 1992)

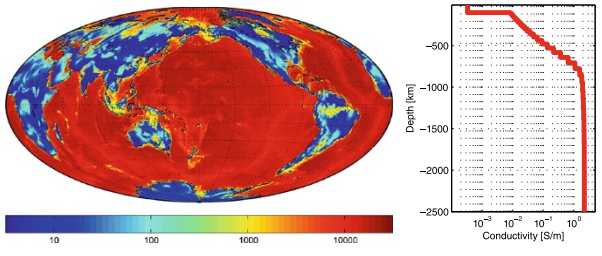

Figure 2 3-D conductivity model. Left: Surface conductance (in S), representing the uppermost 10 km. Right: 1-D conductivity profile beneath the surface shell.

$$\mathbf{E}^{\mathrm{obs}}(\omega) = \mathbf{G}\mathbf{E}^{\mathrm{mod}}(\omega), \quad \mathbf{G} = \begin{pmatrix} G_{xx} & G_{xy} \\ G_{yx} & G_{yy} \end{pmatrix}. \tag{5}$$

G is the frequency-independent, real-valued distortion matrix. Due to these properties, Equation 5 is also valid in time domain, in which it reads

$$\mathbf{E}^{\mathrm{obs}}(t) = \mathbf{G}\mathbf{E}^{\mathrm{mod}}(t). \tag{6}$$

Having the observatory data and the calculated electric fields obtained with the method described in the previous subsection, we can solve the linear system of equations given by Equation 6 for **G**. Since **G** is time-independent, the system is highly over-determined, as the relation must hold for every sample in time. We solve Equation 6 with iteratively re-weighted least squares (e.g. Aster et al. 2005).

We want to note that the issue of estimating the distortion matrix at a geomagnetic observatory was recently also addressed by Love and Swidinsky (2014). In contrast to us, the authors employed a local approach, i.e. they did not describe the structure of the source field. Additionally, the authors used a homogeneous half space instead of a 3-D conductivity model. We will compare the results of both studies later in this paper.

Results and discussion

We consider a large-scale magnetospheric source, which we parametrize with 15 low-degree SHE coefficients $\varepsilon_n^m(\omega)$ ($n \leq 3$, $|m| \leq 3$). We estimate the time spectra of these coefficients separately for all six magnetic storms summarized in Table 1. These are used to synthesize the time series of the electric field at the measurement sites in Japan and the Philippine Sea shown in Figure 1.

As widely known, geomagnetic and geoelectric fields are in magnetic quiet times dominated by the daily solar quiet (*Sq*) variations, which cannot fully be described by our chosen set of coefficients (e.g. Schmucker 2013). To minimize the influence of *Sq*, we estimate distortion matrices from 3-day segments of the calculated and observed time series, which are centred around the magnetic storm of interest.

Ocean bottom observatories

The magnetic storm of April 2000 was the only significant event during the deployment of the ocean bottom electro-magnetometers. For the chosen 3-day segment around this storm, only 4 stations (OB1, OB2, OB5 and OB6) collected trustworthy data. We present observed and predicted electric field at these sites in Figure 3. Note that the 'predicted' electric field is given by $\mathbf{G}\mathbf{E}^{\mathrm{mod}}(t)$. Our estimates of the distortion matrix **G** are presented in Table 2.

Since little galvanic distortion is expected for ocean bottom sites, we assumed **G** to be close to the identity matrix.

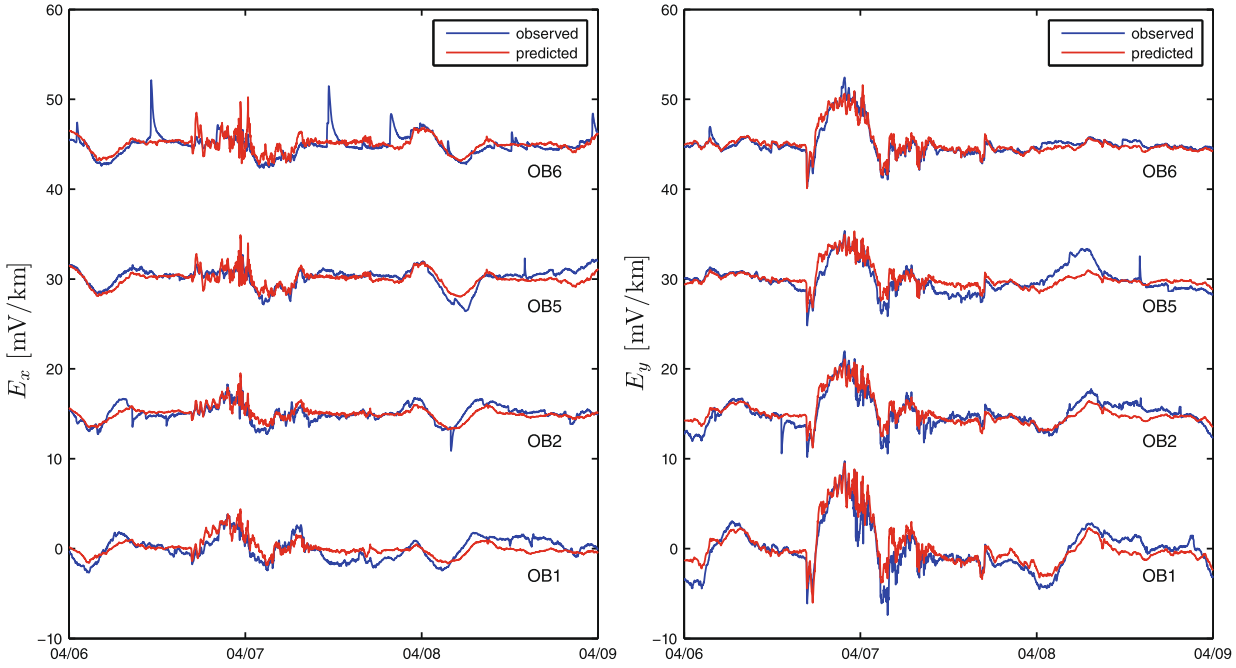

Figure 3 E-field at ocean bottom observatories. Observed (blue) and predicted (red) electric field for the April 2000 magnetic storm. Left panel: E_x; right panel: E_y. Note that the time series at individual stations are shifted by 15 mV/km for clarity.

Indeed, the results at most sites show diagonal elements G_{xx} and G_{yy} close to 1 and off-diagonal elements G_{xy} and G_{yx} close to 0. G_{xx} at OB6 deviates significantly from its expected values; however, E_x^{obs} at OB6 shows a number of non-physical spikes; hence, this deviation might be due to data quality. At OB5, both G_{xx} and G_{yx} deviate clearly from the expected value, indicating that the assumption of a homogeneous layered subsurface might not hold for this station. In general, the results confirm that for oceanic sites the amplitudes of our modellings are close to those of the actual electric field and thus validate the concept of Püthe and Kuvshinov (2013).

In the last two columns of Table 2, we present coefficients of determination. R_x^2 measures how well E_x^{obs} correlates with the inputs E_x^{mod} and E_y^{mod}, while R_y^2 measures how well E_y^{obs} correlates with these inputs. Acceptable coefficients of determination are obtained for all stations, especially in the E_y component.

Table 2 Distortion matrices estimated for ocean bottom stations, using data of the April 2000 magnetic storm

Station	G_{xx}	G_{xy}	G_{yx}	G_{yy}	R_x^2	R_y^2
OB1	0.90	0.46	−0.13	1.13	0.52	0.84
OB2	1.24	0.26	−0.09	0.78	0.63	0.78
OB5	1.70	−0.15	−0.59	1.02	0.64	0.70
OB6	2.04	−0.40	−0.12	1.34	0.68	0.91

Onshore observatories

The onshore observatories KAK, KNY and MMB provide continuous time series of the electric field. We estimate distortion matrices separately for each magnetic storm. This permits us to investigate the robustness of our estimates. Tables 3, 4 and 5 contain the estimated elements of **G** for each storm as well as mean value and standard deviation, obtained by analysis of all events. The pronounced differences between the estimates obtained at different sites are noteworthy. At KAK (Table 3), G_{yy} is large compared to all other elements, while at MMB (Table 5), G_{xx} and G_{xy} are large. Maximum values for both observatories are around 3, indicating that our modellings underestimate the amplitude of the actual electric field by about this factor. At KNY (Table 4), in contrast, all elements are < 1, indicating that our modellings overestimate the amplitude of the electric field. These very different results confirm that galvanic distortion is a very local phenomenon.

A look at the variance between individual events reveals that the estimates of **G** are quite robust. Except for a few elements (such as G_{yx} at KAK), the standard deviations have clearly smaller amplitudes than the estimates themselves. Coefficients of determination are relatively stable over different storms but vary significantly with site and component. Highest R_x^2 and R_y^2 are obtained for KAK; at MMB, they are comparably low. In this context, we want to stress again that our analysis is based on a small number of low-degree source terms. While these terms can

Table 3 Distortion matrix and statistics for observatory KAK

Storm	G_{xx}	G_{xy}	G_{yx}	G_{yy}	R_x^2	R_y^2
Apr-00	0.27	1.05	0.21	3.66	0.90	0.93
Jul-00	0.20	1.00	−0.29	3.11	0.89	0.92
Aug-00	0.12	0.86	−0.40	3.00	0.81	0.90
Mar-01	0.17	0.83	−0.16	3.24	0.76	0.91
Oct-03	−0.15	0.73	−0.91	2.60	0.76	0.81
Nov-03	0.12	0.92	−0.50	3.55	0.94	0.94
Mean	0.12	0.90	−0.34	3.19	0.84	0.90
Standard deviation	0.15	0.12	0.37	0.39	0.08	0.05

Table 5 Distortion matrix and statistics for observatory MMB

Storm	G_{xx}	G_{xy}	G_{yx}	G_{yy}	R_x^2	R_y^2
Apr-00	2.60	3.67	0.43	1.14	0.62	0.34
Jul-00	2.44	3.84	0.31	1.19	0.80	0.70
Aug-00	1.80	1.98	0.03	0.99	0.51	0.63
Mar-01	2.32	2.46	0.25	0.92	0.60	0.59
Oct-03	1.24	2.02	0.08	0.99	0.41	0.49
Nov-03	2.90	4.00	0.31	0.89	0.89	0.77
Mean	2.22	2.99	0.23	1.02	0.64	0.59
Standard deviation	0.60	0.94	0.15	0.12	0.18	0.15

likely reproduce variations in the large-scale magnetospheric ring current, they cannot fully describe the daily *Sq* variations, which are always present in the data.

In Figures 4, 5 and 6, we compare the observed and the predicted electric field for the October 2003 magnetic storm (also known as the 'Halloween storm') at observatories KAK, KNY and MMB. Note again that in these figures, the 'predicted' electric field is given by $\mathbf{GE}^{\mathrm{mod}}(t)$. The plotted time series reflect the different correlations between measurements and model predictions at different observatories. While the observed electric field at KAK and KNY is excellently reproduced, observations and predictions at MMB differ in detail. The peak amplitudes and the overall shape of the time series are however also well-reproduced at MMB.

If comparing the results obtained for different storms, the October 2003 event stands out, both in the estimates of $\mathbf{G}$ (e.g. G_{xx}, G_{yx} and G_{yy} at KAK; G_{xx} at MMB) and in the coefficients of determination (e.g. comparably small R_y^2 at KAK and R_x^2 at MMB). These findings might indicate a violation of our assumption that the source can be described by a moderate number of low-degree spherical harmonics. This could be due to an extension of the auroral oval well beyond its usual position equatorward as far as Japan. For particularly strong magnetic storms such as the October 2003 event, the accuracy of our method might thus be limited even in the mid-latitudes.

Table 4 Distortion matrix and statistics for observatory KNY

Storm	G_{xx}	G_{xy}	G_{yx}	G_{yy}	R_x^2	R_y^2
Apr-00	0.42	−0.24	−0.19	0.78	0.72	0.82
Jul-00	0.54	−0.19	−0.70	0.66	0.68	0.86
Aug-00	0.53	−0.09	−0.65	0.56	0.60	0.91
Mar-01	0.62	−0.17	−0.55	0.70	0.85	0.91
Oct-03	0.34	0.26	−0.57	0.97	0.71	0.90
Nov-03	0.55	0.24	−0.60	1.04	0.65	0.95
Mean	0.50	−0.03	−0.54	0.78	0.70	0.89
Standard deviation	0.10	0.23	0.18	0.19	0.08	0.05

Galvanic and inductive effects

In this section, we investigate the importance of 3-D modelling for our analysis and, in particular, address the question if galvanic and inductive effects are correctly separated. Throughout the section, we will, as an example, focus on the distortion matrix at KAK for the October 2003 storm.

To test the importance of 3-D modelling, we repeat the above simulations in a 1-D model. For depths >10 km, this model is equivalent to the 3-D model, but the heterogeneous top layer is replaced by a homogeneous shell with the conductivity of the area around the specific observatory, picked from the surface conductance map. With this 1-D model, we obtain for KAK and the October 2003 storm

$$\mathbf{G}_{1-\mathrm{D}}^{\mathrm{KAK}} = \begin{pmatrix} -0.19 & 0.55 \\ -1.16 & 1.89 \end{pmatrix}, \tag{7}$$

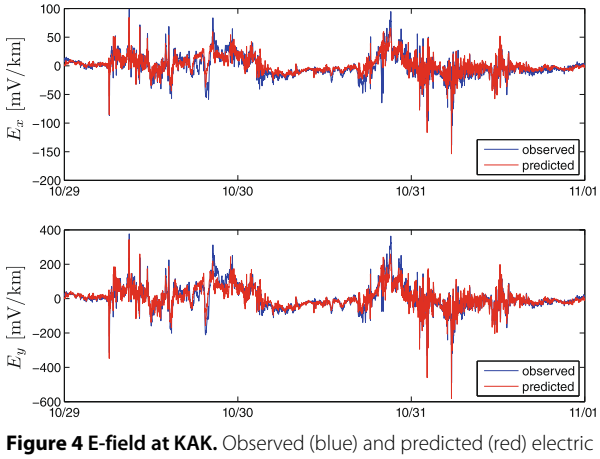

Figure 4 E-field at KAK. Observed (blue) and predicted (red) electric field for the October 2003 (Halloween) magnetic storm. Top panel: E_x; bottom panel: E_y.

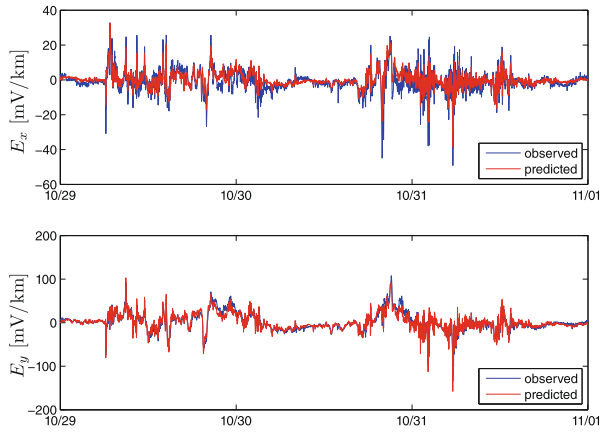

Figure 5 E-field at KNY. Observed (blue) and predicted (red) electric field for the October 2003 magnetic storm.

with $R_x^2 = 0.23$ and $R_y^2 = 0.24$. Similar results are obtained with data of the other storms; the averaged coefficients of determination are $R_x^2 = 0.46$ and $R_y^2 = 0.47$ and thus considerably smaller than those obtained with 3-D modelling ($R_x^2 = 0.84$, $R_y^2 = 0.90$, cf. Table 3). The estimated distortion matrix however is not too different from that obtained with 3-D modelling,

$$\mathbf{G}_{3-\mathrm{D}}^{\mathrm{KAK}} = \begin{pmatrix} -0.15 & 0.73 \\ -0.91 & 2.60 \end{pmatrix}. \tag{8}$$

One-dimensional modelling for KNY also results in a drop in R_x^2 and R_y^2 but more pronounced changes in the elements of **G**, while 1-D modelling for MMB results in similar coefficients of determination and a very different distortion matrix. For the ocean bottom observatories, we finally obtain similar coefficients and minor differences in **G** for 1-D and 3-D modellings. This leads to the following conclusions:

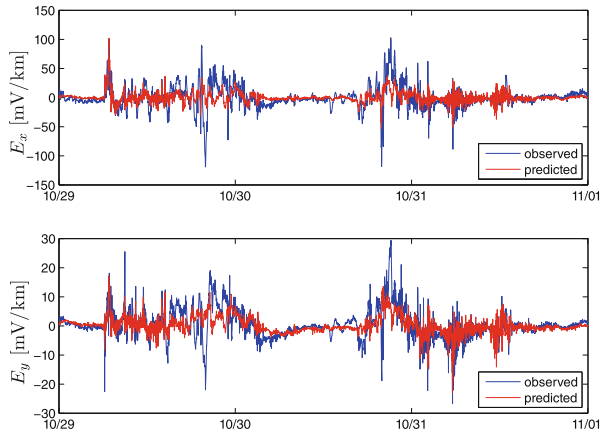

Figure 6 E-field at MMB. Observed (blue) and predicted (red) electric field for the October 2003 magnetic storm.

1. In regions in which the conductivity structure is mostly 1-D (such as the Philippine Sea), 3-D modelling has only minor effects on the results.
2. In coastal regions (such as the locations of all three observatories in Japan), 3-D modelling is crucial to correctly predict the shape of electric field time series during a magnetic storm, indicated by good correlations between observations and model predictions.
3. For some locations (such as MMB), modelled inductive and galvanic effects can compensate each other in their effect on the calculated electric field. One-dimensional modelling yields similar coefficients of determination as 3-D modelling but to the price of an incorrect separation of inductive and galvanic effects, indicated by a very different distortion matrix.

The distortion matrix for KAK was recently also estimated by Love and Swidinsky (2014), using data of the Halloween storm of October 2003. The published results are

$$\mathbf{G}_{\mathrm{L\&S}}^{\mathrm{KAK}} = \begin{pmatrix} 1.33 & 0.42 \\ -0.21 & 0.06 \end{pmatrix}. \tag{9}$$

We do not observe any similarity with our results for the same event ($\mathbf{G}_{3-\mathrm{D}}^{\mathrm{KAK}}$, Equation 8). However, both studies can reliably reproduce the measured time series of both E_x and E_y. Indeed, Love and Swidinsky (2014) state that they can reproduce 87% of the measured variations (although it is not entirely clear from the description how this value is calculated). We reach coefficients of determination of 76% for E_x and 81% for E_y.

To test whether the differences in the estimated distortion matrices are caused by the differences in the conductivity models, we repeat our above simulations once again in a homogeneous half-space model with conductivity of 5.13×10^{-4} S/m. This value was co-estimated (together with the distortion matrix) by Love and Swidinsky (2014). With this model, we obtain for KAK and the October 2003 storm

$$\mathbf{G}_{\mathrm{homog.}}^{\mathrm{KAK}} = \begin{pmatrix} -0.04 & 0.34 \\ -0.44 & 1.24 \end{pmatrix}, \tag{10}$$

with $R_x^2 = 0.47$ and $R_y^2 = 0.48$. This result is markedly different from $\mathbf{G}_{3-\mathrm{D}}^{\mathrm{KAK}}$ but also from $\mathbf{G}_{\mathrm{L\&S}}^{\mathrm{KAK}}$. Thus, although using the same conductivity model, the distortion matrices estimated by Love and Swidinsky (2014) and by us do not agree. A possible explanation for this disagreement is the different handling of the source. While Love and Swidinsky (2014), using the impedance tensor, implicitly assume a plane-wave source as common in MT, we derive the actual structure of a large-scale, heterogeneous source field.

Towards real-time prediction

We finally want to investigate whether our method is suitable for real-time prediction of the electric field during magnetic storms. To this purpose, we need to know the temporal evolution of the source field prior to the arrival of the storm. This requires some simplifications. As widely known, the dominant source of induction in the mid-latitudes is a symmetric ring current in the magnetosphere, described spatially by the spherical harmonic $Y_1^0 = \cos\vartheta$ and temporally by the corresponding coefficient ε_1^0. The latter can approximately be related to the *Dst* index as (Olsen and Kuvshinov 2004)

$$\varepsilon_1^0 \approx \frac{-Dst}{1+\tilde{Q}}, \tag{11}$$

with $\tilde{Q} = 0.27$ being a first-order correction for induction effects (Langel and Estes 1985).

A forecast of *Dst* is possible from analysis of solar wind observations by the Advanced Composition Explorer (ACE) satellite at the L1 Lagrange point (Temerin and Li 2002). Depending on the solar wind speed, the *Dst* forecasts are available approximately 1 h in advance. Moreover, an approximate 6-day-forecast for *Dst*, which is based on direct solar observations, was recently presented by Tobiska et al. (2013).

In this study, we use the *Dst* forecast from ACE observations for the October 2003 magnetic storm and calculate ε_1^0 with Equation 11. The result is compared to ε_1^0 obtained with our method in the lower panel of Figure 7. The overall shapes of observed and predicted time series are in good agreement, and the maximum amplitudes are well-predicted, too. The offset in the recovery phase might be due to the use of Equation 11, which does not account for the time lag due to inductive effects. The most prominent difference however are the rapid oscillations of ε_1^0, which are present in the time series derived with our method, but not in that predicted from ACE observations. The *Dst* forecast has a nominal temporal resolution of 10 min, but it only correctly reproduces features on time scales of hours. This is also apparent from the power spectra, shown in the upper panel of Figure 7. For periods shorter than a few hours, the *Dst* forecast lacks energy.

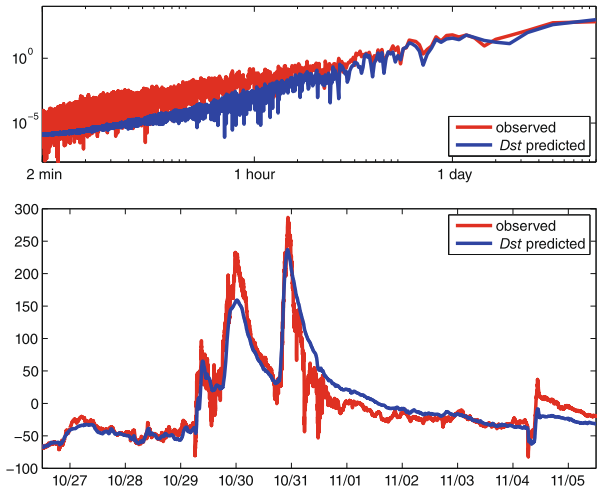

Figure 7 Power spectra (upper panel) and time series (lower panel) of ε_1^0. Red: estimated from observatory magnetic data; blue: predicted from solar wind parameters with the method of Temerin and Li (2002).

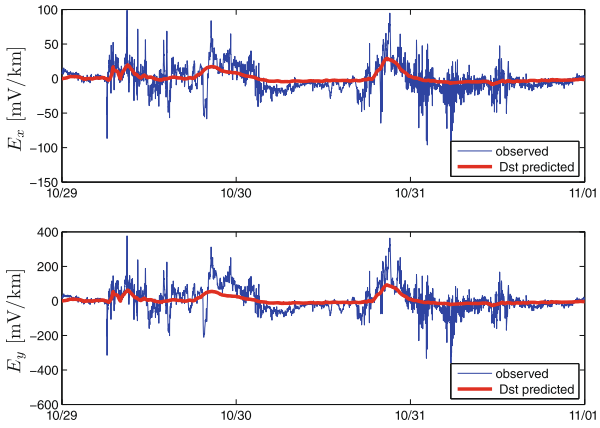

Figure 8 E-field at KAK - revisited. Observed electric field (blue) and electric field predicted from the *Dst* forecast (red) for the October 2003 magnetic storm.

We use the responses of our 3-D model, the estimated distortion matrix for KAK (mean values, cf. Table 3) and the *Dst* prediction of ε_1^0 to compute the electric field at KAK for the October 2003 storm. The results are shown in Figure 8. The agreement between observations and predictions is weak. Only the very broad features of the variation of the electric field during the storm are correctly reproduced. Peak amplitudes do not match, and the characteristic fast oscillations are missing. We think that this is mostly due to the limited temporal resolution of the *Dst* forecast. The electric field undergoes very rapid oscillations during magnetic storms, which can only be reproduced if the temporal evolution of the source field on the same time scales is known.

Conclusions

In this study, we revisited the method of Püthe and Kuvshinov (2013) to calculate the electric field generated in mid-latitude regions during magnetic storms. The method involves 3-D modelling of induction processes in a heterogeneous Earth and the construction of a source model described by low-degree spherical harmonics from observatory magnetic data.

We extended the work of Püthe and Kuvshinov (2013) by investigating the fit of the modellings with electric field

measurements at ocean bottom stations in the Philippine Sea and at onshore observatories in Japan. Observations and modellings are linearly related by a distortion matrix, which accounts for galvanic effects. We reliably determined such matrices with, dependent on site and component, coefficients of determination between 0.59 and 0.90. The largest matrix elements reach values around 3, indicating that the modellings underestimate the actual electric field by about this factor. However, since galvanic distortion is a very local phenomenon, it is not possible to draw conclusions from this finding on global electric field models as presented by Püthe and Kuvshinov (2013).

The results of this study also stress the need for 3-D modelling. Correlations between observations and predictions are markedly higher if the latter are generated in a 3-D model. In addition, a correct separation of galvanic and inductive effects is only possible with a precise 3-D model. We do not claim that our model fulfils this requirement, as in the considered period range, inductive effects take place at scale lengths that are significantly smaller than its resolution. Nevertheless, the inclusion of a heterogeneous surface shell is a clear improvement to a 1-D model - and our method can easily incorporate more complex conductivity models as soon as they are available, such as that currently developed by Alekseev et al. (2014). Using responses of a more complex model will not have any effect on the computational cost, because these responses are independent of the source and can therefore be computed beforehand and archived.

In a larger framework, this study can be seen as contribution to a procedure that predicts the hazard to technological systems in mid-latitude regions due to geomagnetic disturbances. By computing the electric field on the Earth's surface, our method bridges the gap between predictions of geomagnetic disturbances (e.g. Temerin and Li 2002; Tobiska et al. 2013) and calculations of the currents induced in conductor networks (e.g. Lehtinen and Pirjola 1985). To establish a real-time forecast system for GIC, it will be necessary to connect and automate the existing individual algorithms. In addition, as shown in this study, a more precise forecast of the temporal evolution of the source field is crucial for a correct prediction of fast fluctuating electric fields.

As already discussed by Püthe and Kuvshinov (2013), the formalism presented above could in principle also be applied to magnetic substorms, which cause the strongest EM signals in polar latitudes and are due to intensifications of the auroral current system. This will however require a precise description of the auroral source, which is extremely variable both in space and time, and connected with this, a more local approach involving a different set of basis functions.

Finally, we would like to note that the described formalism to estimate distortion matrices could also be applied in MT. If sufficiently long time series, containing magnetic storms, are collected, the method outlined in this paper can be used to correct for the static shift.

Abbreviations

ACE: Advanced Composition Explorer (satellite); *Dst*: disturbed storm time; EM: electromagnetic; GIC: geomagnetically induced currents; MT: magnetotellurics; SHE: spherical harmonic expansion.

Competing interests

The authors declare that they have no competing interests.

Authors' contributions

CP performed 1-D and 3-D modellings and drafted the manuscript. CM collected the data and estimated distortion matrices. AK initiated the study, provided the 3-D modelling code and assisted in the scientific work. All authors contributed to elaborating the numerical codes specific to this study, read and approved the final manuscript.

Acknowledgements

The authors express their gratitude to the staff of the geomagnetic observatories who have collected and distributed the data. Magnetic data were downloaded from the World Data Center for Geomagnetism, Kyoto (http://wdc.kugi.kyoto-u.ac.jp). Electric data of the Japanese stations were downloaded from the Kakioka Magnetic Observatory (http://www.kakioka-jma.go.jp/en). Data of the ocean bottom survey were downloaded from the Earthquake Research Institute, University of Tokyo (http://ohpdmc.eri.u-tokyo.ac.jp). The *Dst* forecast was downloaded from the Laboratory for Atmospheric and Space Physics, University of Colorado Boulder (http://lasp.colorado.edu/home/spaceweather/). All data are freely available for non-commercial use. This work has been supported by the Swiss National Science Foundation under grant no. 2000021-140711/1 and in part by the Russian Foundation for Basic Research under grant no. 13-05-12111.

Author details

[1]Institute of Geophysics, ETH Zürich, Sonneggstrasse 5, 8092 Zürich, Switzerland. [2]CIRES and NOAA's NGDC, University of Colorado, Boulder, USA.

Received: 19 September 2014 Accepted: 22 November 2014
Published online: 23 December 2014

References

Alekseev D, Kuvshinov A, Palshin N (2014) Compilation of 3-D global conductivity model of the Earth for space weather applications. Earth Planets Space (this issue)

Aster R, Borchers B, Thurber C (2005) Parameter estimation and inverse problems. Elsevier Academic Press, Waltham (MA), USA

Chave A, Jones A (2012) The magnetotelluric method. Cambridge University Press, Cambdrige, UK

Daglis I(ed.) (2004) Effects of space weather on technology infrastructure. Kluwer Academic Publishers, Dordrecht, NL

Groom R, Bahr K (1992) Corrections for near-surface effects: decomposition of the magnetotelluric impedance tensor and scaling corrections for regional resistivities: a tutorial. Surv Geophys 13:341–379

Jiracek G (1990) Near-surface and topographic distortions in electromagnetic induction. Surv Geophys 11:163–203

Kappenman J (2005) An overview of the impulsive geomagnetic field disturbances and power grid impacts associated with the violent Sun-Earth connection events of 29–31 October 2003 and a comparative evaluation with other contemporary storms. Space Weather 3. doi:10.1029/2004SW000128

Kuvshinov A (2008) 3-D global induction in the oceans and solid Earth: recent progress in modeling magnetic and electric fields from sources of magnetospheric, ionospheric and oceanic origin. Surv Geophys 29:139–186. doi:10.1007/s10712-008-9045-z

Kuvshinov A, Olsen N (2006) A global model of mantle conductivity derived from 5 years of CHAMP, Ørsted, and SAC-C magnetic data. Geophys Res Lett 33. doi:10.1029/2006GL027083
Kuvshinov A, Semenov A (2012) Global 3-D imaging of mantle electrical conductivity based on inversion of observatory C-responses – I. An approach and its verification. Geophys J Int 189:1335–1352. doi:10.1111/j.1365-246X.2011.05349.x
Langel R, Estes R (1985) Large-scale, near-Earth magnetic fields from external sources and the corresponding induced internal field. J Geophys Res 90:2487–2494
Lehtinen M, Pirjola R (1985) Currents produced in earthed conductor networks by geomagnetically-induced electric fields. Ann Geophys 4:479–484
Love J, Chulliat A (2013) An international network of magnetic observatories. Eos Trans AGU 42:373–374
Love J, Swidinsky A (2014) Time causal operational estimation of electric fields induced in the Earth's lithosphere during magnetic storms. Geophys Res Lett 41:2266–2274. doi:10.1002/2014GL059568
Minamoto Y (2013) Availability and access to data from Kakioka magnetic observatory. Japan. Data Sci J 12:30–35
Manoj C, Kuvshinov A, Maus S, Lühr H (2006) Ocean circulation generated magnetic signals. Earth Planets Space 58:429–437
Olsen N, Kuvshinov A (2004) Modeling the ocean effect of geomagnetic storms. Earth Planets Space 56:525–530
Pulkkinen A, Bernabeu E, Eichner J, Beggan C, Thomson A (2012) Generation of 100-year geomagnetically induced current scenarios. Space Weather 10. doi:10.1029/2011SW000750
Püthe C, Kuvshinov A (2013) Towards quantitative assessment of the hazard from space weather Global 3-D modellings of the electric field induced by a realistic geomagnetic storm. Earth Planets Space 65:1017–1025. doi:10.5047/eps.2013.03.003
Seama N, Baba K, Utada H, Toh H, Tada N, Ichiki M, Matsuno T (2007) 1-D electrical conductivity structure beneath the Philippine Sea: results from an ocean bottom magnetotelluric survey. Phys Earth Planet Int 162:2–12. doi:10.1016/j.pepi.2007.02.014
Schmucker U (2013) A spherical harmonic analysis of solar daily variations in the years 1964-1965: response estimates and source fields for global induction — I. Methods. Geophys J Int 136:439–454
Simpson F, Bahr K (2005) Practical Magnetotellurics. Cambridge University Press, Cambdrige, UK
Temerin M, Li X (2002) A new model for the prediction of *Dst* on the basis of the solar wind. J Geophys Res 107. doi:10.1029/2001JA007532
Tobiska W, Knipp D, Burke W, Bouwer D, Bailey J, Odstrcil D, Hagan M, Gannon J, Bowman B (2013) The *Anemomilos* prediction methodology for Dst. Space Weather 11. doi:10.1002/swe.20094
Viljanen A, Pirjola R (1994) Geomagnetically induced currents in the Finnish high-voltage power system. a geophysical review. Surv Geophys 15:383–408